ChemComm

COMMUNICATION

View Article Online
View Journal | View Issue

Cite this: *Chem. Commun.*, 2024, **60**, 7594

Received 15th April 2024,
Accepted 26th June 2024

DOI: 10.1039/d4cc01781a

rsc.li/chemcomm

Inverse opals with reactive surface chemistry as sensors for aqueous pollutants†

Giulia Magnabosco,[a] Maria Ochs,[b] Natalie Bonakdar,[a] Laura Czerwenka,[b] Annette Andrieu-Brunsen*[b] and Nicolas Vogel*[a]

Inverse opal colorimetric sensors operating on wetting transitions usually rely on physical differences of the infiltrating liquid. Here, we exploit a reactive surface chemistry that changes wettability upon binding of an analyte. Upon binding of Fe^{3+} to a Schiff base immobilized on the porous structure, the surface becomes more hydrophilic, triggering the infiltration of the structure and causing the structural color to disappear.

The detection of dissolved species in aqueous solutions is of relevance in a wide variety of fields, ranging from water management and pollutant detection[1–3] to healthcare.[4,5] Typically, such analyses rely on complex, multistep procedures conducted in specialized laboratories with sophisticated infrastructure. The possibility to monitor the analyte of interest *in situ* is attracting growing interest as a convenient and direct point of care diagnostic.[6,7] Ideally, the presence of dissolved species is directly encoded *via* an autonomous, detectable response of a material.

Various concepts for the solid-state detection of water pollutants have been established. For example, the change in color upon binding of an analyte to a dye immobilized on solid supports can be used for sensing.[8] Colorimetric sensors based on photonic crystals enable direct modification of their structural coloration by changes triggered either in the structural arrangement or in the refractive index of their components.[9,10] The structural coloration generated by thin film interference of polymeric films can be used for sensing when the film shrinks or swells in the presence of the analyte.[11] 3D colloidal photonic crystals, commonly referred to as opals, show structural color because of the periodic arrangement of their constituent particles. For opals embedded in polymer matrices, a color change can be observed when the matrix swells by interacting with an analyte and changes the distance between the particles.[12–15]

Inverse opals (IOs), three-dimensional porous networks with fully interconnected, uniform pores, exhibit structural coloration visible by the naked eye due to the periodic nature of the nanopores.[16–20] When prepared using a matrix able to shrink upon interaction with an analyte, they can also act as colorimetric sensors.[21] Since structural coloration relies on a refractive index contrast between pore and matrix,[16] the infiltration of an IO with liquid eliminates the observable coloration because of the higher refractive index of liquids compared to air.[16,18,22–25] This constitutes a simple, binary read-out of the wetting state.

The regularity and interconnected nature of the nanopores in an IO induces a well-defined wetting transition that depends on the contact angle of a given liquid with the pore walls.[19,22,23,26–28] The pores remain unwetted if the contact angle θ is larger than the pore opening angle ϑ (Fig. 1).[24,27] Only for $\theta < \vartheta$ will the liquid be able to penetrate through the neck and propagate into the porous network. The underlying reason for this change in pore filling is a change in the shape of the meniscus the liquid forms at the necks of the pores (Fig. 1b and c).[24,27]

This defined wetting transition is the key for an autonomous colorimetric sensor. When the surface chemistry of the IO is adjusted in a way that the contact angles of two different liquids are above and below the neck opening angle, one liquid will infiltrate the IO, while the other one cannot infiltrate the pore network (Fig. 1b–e).[27] The associated loss of structural color thus unambiguously indicates the presence of the first liquid.

This concept has enabled the wetting-based discrimination between different alcohol species (*i.e.* methanol, ethanol, isopropanol), different alcohol contents,[22,24] or between regular gasoline and diesel.[24] Recently, IOs have also been exploited to pre-screen newborns for jaundice by exploiting changes in the surface tension in urine, allowing for easy, at-home monitoring of the development of this common condition.[23]

To this point, however, the wetting transition has been mainly limited to triggers provided by the physical properties of the liquids themselves, such as their surface tension. Since

[a] *Institute of Particle Technology Friedrich-Alexander-Universität Erlangen-Nürnberg Cauerstraße 4, 91058 Erlangen, Germany. E-mail: nicolas.vogel@fau.de*
[b] *Ernst-Berl Institut für Technische und Makromolekulare Chemie Technische Universität Darmstadt Alarich-Weiss-Str. 8 64287 Darmstadt, Germany. E-mail: annette.andrieu-brunsen@tu-darmstadt.de*

† Electronic supplementary information (ESI) available: Experimental methods and further characterization. See DOI: https://doi.org/10.1039/d4cc01781a

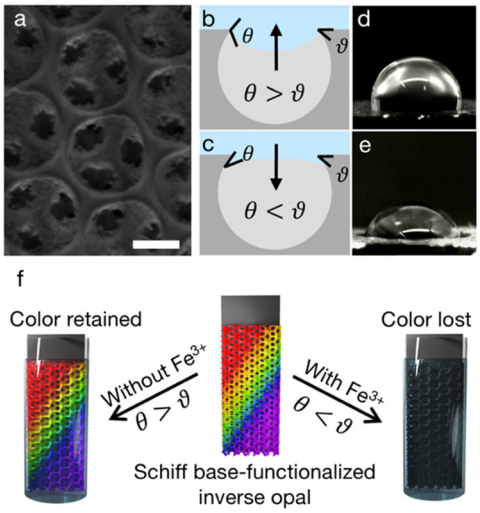

Fig. 1 Schematic of the operation principle of an inverse opal-based autonomous sensor. (a) SEM image of an IO. Scalebar is 200 nm. When the contact angle θ is larger than the pore opening angle ϑ, the structure does not wet (b) and (d). When the contact angle θ is smaller than the pore opening angle ϑ, the structure wets (c) and (e). (f) The Schiff base-functionalized inverse opal changes its wettability upon interaction with Fe^{3+} and it wets, suppressing the structural color.

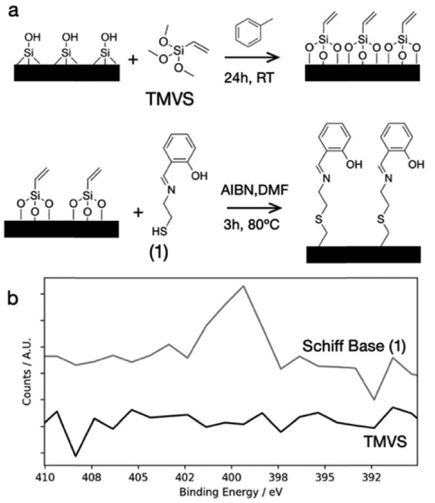

Fig. 2 Schematic of the functionalization of the silica surface with the Schiff base. (a) 1- The surface is activated using O_2 plasma. 2- The surface is functionalized with trimethoxyvinilsilane (TMVS). 3- The Schiff base is bound to the surface with a thiol–ene reaction. (b) XPS spectra of the nitrogen signal before (black) and after (gray) the binding of the Schiff base (1).

soluble analytes generally do not influence the surface tension of the liquid, the wetting transition cannot be triggered by the presence of the analyte itself. Therefore, the change in contact angle must be induced by an *in situ* change of the chemistry of the surface, rather than by a change in the property of the liquid. Such a reactive surface chemistry must provide selective recognition units that trigger a change in wettability upon binding of the analyte. When introduced within the porous structure of the IO, this binding can therefore favor the wetting of the previously unwetted IO in the presence of the analyte (Fig. 1f).

Here, we develop this new sensing strategy based on a change in wettability in the surface of the IO upon interaction with an analyte, namely the chelation of a metal ion. We devise a reaction scheme to create reactive surface chemistries based on half-Salen Schiff bases, successfully functionalize the inner pore surface of IOs, investigate the change in wettability induced by the binding of Fe^{3+} as a model ion, and demonstrate that this change in wettability can trigger a wetting transition to successfully provide a colorimetric read-out of the binding event.

We identify Schiff bases as a candidate for such a reactive surface chemistry, as their complexation capacities to different metal ions can be tailored *via* their molecular structure.[29–31] Salen motives, a particular type of Schiff bases containing two acidic hydroxyls[26–28] and two aryl-imine groups,[32] can act as bidentate ligands for a variety of metal ions through the donation of the electron lone pair of the azomethine nitrogen.[32] Salen motives have already been used to develop sensors to detect a variety of metal ions,[33–37] typically by exploiting a change in the photochemical behavior of the ligands. Half-Salen motives, only consisting in one acidic hydroxyl aryl-imine group, can still coordinate metals, and allow for water molecules to complete the coordination sphere of the bound metal. This may in turn increase the hydrophilicity of a surface onto which such a compound is bonded.

We start the design of the autonomous colorimetric sensors by preparing IOs as porous photonic crystals that provide the structural color-based detection signal. We use the colloidal co-assembly method[18] with 340 nm polystyrene colloidal particles, which enables the fabrication of nearly crack-free, well-ordered silica IOs that exhibit visible structural coloration from the periodic arrangement of the nanopores (Fig. S1a–d, ESI†). A low number of cracks and the interconnectivity of the pores (Fig. 1a and Fig. S1a, ESI†) are the prerequisite for observing a sharp wetting transition.[19,38] We calculate the pore opening angle from SEM images (Fig. S1d, ESI†) to be around $20^\circ \pm 2^\circ$.

Next, we devise a reactive surface chemistry able to trigger a change in substrate wettability upon the binding of a target analyte. We synthesize (*E*)-2-(((2-mercaptoethyl)imino)methyl)-phenol (**1**), a half-Salen Schiff base. This Schiff base was selected as it shows a promising selectivity towards the binding of Fe^{3+} ions, as observed by the change in the UV-vis spectra upon the formation of the complex in solution (Fig. S2, ESI†).

The successful surface functionalization is confirmed by X-ray photoelectron spectroscopy (XPS), where the nitrogen signal is visible after the immobilization of the Schiff-base on the surface (Fig. 2b). When a hexavalent metal is coordinated by the Schiff-base (1), it can still coordinate 4 additional water molecules, thereby increasing the water wettability of the surface (Fig. 3a).

For binding (**1**) to the IO silica surface, we use the thiol functionality integrated in the Schiff base as anchor group. To this end, we first create a monolayer of surface-bound vinyl-silane groups *via* silane chemistry. Subsequently, we employ thiol–ene chemistry to bind the Schiff base to the double bond, thus creating the reactive surface coating (Fig. 2a).[39]

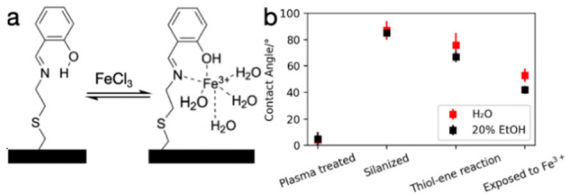

Fig. 3 Wetting behavior of functionalized surface. (a) Suggested mechanism for increased wettability upon interaction with Fe^{3+}. (b) Contact angles measured on a flat surface with a 20% EtOH solution (black) or water (red) at different steps of the functionalization procedure and after interaction with Fe^{3+}.

We investigate the change in surface wettability using water contact angle (WCA) measurements on a planar glass slide (Fig. 3b, red squares). The initially hydrophilic glass surface (WCA $< 20^\circ$) is rendered more hydrophobic by the introduction of the vinyl functionalities of the trimethoxyvinylsilane (TMVS) (WCA = $87^\circ \pm 7^\circ$). The binding of the Schiff base (1) lowers the hydrophobicity to a WCA of $76^\circ \pm 9$ °C, reflecting the presence of the phenolic OH group.

When placed in contact with a solution of Fe^{3+} (60% EtOH, 5 mM, 1 hour), the hydrophilicity of the surface is significantly increased, evidenced by a decrease in WCA to $53^\circ \pm 5$.

The contact angle can be further adjusted by mixing the aqueous solution with ethanol. For example, using a 20% ethanolic water solution, the CA on the Schiff base functionalized flat surface is lowered from $67^\circ \pm 4^\circ$ to $42^\circ \pm 3^\circ$ in the presence of Fe^{3+} (Fig. 3b, black squares). This control is important to match the CA with the wetting transition of the IO. Note that changing the pore structure of the inverse opal itself could be used similarly to match the wetting transition to the CAs of the reactive surface. We now incorporate the reactive surface chemistry into the porous network of the IO (Fig. 4). We first establish that a surface-functionalized IO in the absence of Fe^{3+} ions is not wetted by water containing 20% ethanol, as seen by the intense structural color of the sample (Fig. 4). We demonstrate the ability to trigger a wetting transition *via* the binding of a dissolved analyte as follows. We expose the reactive surface chemistry of the IO to a 5 mM Fe^{3+} solution in 60% EtOH, which has a sufficiently small CA (CA $< 20^\circ$) that the liquid infiltrates the IO. After 60 min, we wash and dry the sample. When exposed to a 20% ethanol solution, this sample is now wetted, evidenced by the disappearance of the structural color (Fig. 4a and b). This simple visual observation is corroborated by reflectance spectra of the two samples, where the photonic stop band of the sample exposed to Fe^{3+} disappears when immersed in the 20% ethanol solution (Fig. 4c).

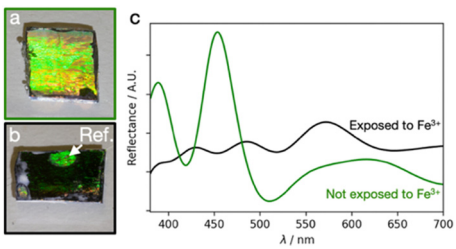

Fig. 4 Colorimetric detection of Fe^{3+} ions from aqueous solutions. (a) Photograph of a Schiff base-functionalized IO exposed to a 20% ethanolic aqueous solution without previous exposure to Fe^{3+}. The structural coloration is clearly observed as the sample is not wetted by the liquid. (b) An IO with the identical surface chemistry exposed to a 20% ethanolic solution previously exposed to a 60% EtOH Fe^{3+} solution is wetted and does not exhibit structural color. Note the colored spot on the top of the sample – indicated by the white arrow - was not exposed to Fe^{3+} by protecting it with an epoxy resin and served as an internal reference. The photographs were collected at a slight angle to emphasize the color. (c) Corresponding reflectance spectra of both samples, showing the suppression of the photonic stop band upon exposure to Fe^{3+} ions.

The wetting behavior implies that the critical contact angle for wetting is in between $\sim 42^\circ$ (as the sample exposed to Fe^{3+} is wetted) and $\sim 67^\circ$ (as the reference sample is not wetted). This experimental threshold differs from the theoretical threshold determined geometrically (Fig. 1). We ascribe these differences to (i) variability in the size of the IO pore measurement, as the value needs to be determined by a projection of a 3D surface on the image plane, (ii) intrinsic roughness of the sample, and (iii) a difference in the functionalization efficiency when performed in the confined, non-planar environment of the nanopore itself.

We assess the selectivity of the reactive surface chemistry by exposing the functionalized IOs to 5 mM solutions of Fe^{2+} and Fe^{3+} for 1 hour (Fig. 5c–f). When the system is exposed to Fe^{2+}, it does not wet and the color is retained (Fig. 5c and d). Only when the sensor is exposed to Fe^{3+}, the structure wets and the color disappears (Fig. 5e and f). The selectivity to Fe^{3+} is caused by the selective complexation of the trivalent ion, as evidenced from the decrease in contact angle. In contrast, the exposure to Fe^{2+} does not decrease the contact angle, indicating that the Schiff base does not complex Fe^{2+} (Fig. S2, ESI†). We also demonstrate the selectivity of the system towards other common metal ions. After exposure to Al^{3+} or Cu^{2+} ions (Fig. 5g–j), no color disappearance is observed.

In conclusion, we demonstrate a new concept for the fabrication of colorimetric photonic crystal sensors based on reactive surface chemistry. We control the wettability of the surface *via* the binding of an analyte, and exploit the wetting transition to provide a simple, unambiguous readout (color *vs.* no color) to detect the presence of this analyte.

In our case, the wetting transition is not triggered by differences in the physical proprieties of the infiltrating liquids, as previously shown in the literature. In this proof of principle,

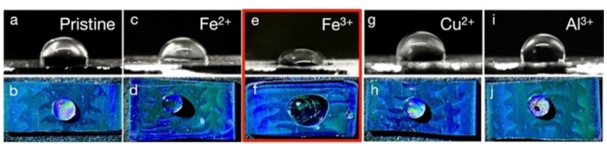

Fig. 5 Selectivity of the reactive surface chemistry towards Fe^{3+}. Side view of a 20% EtOH droplet on a pristine functionalized IO (a), and IOs exposed to Fe^{2+}(c), Fe^{3+} (e), Cu^{2+} (g), and Al^{3+} (i). Top view of a 20% EtOH droplet on a pristine functionalized IO (b), an IO exposed to Fe^{2+} (d) and an IO exposed to Fe^{3+} (f) where the disappearance of structural color can be appreciated, an IO exposed to Cu^{2+} (h), an IO exposed to Al^{3+} (j).

we trigger the wetting transition by the complexation Fe^{3+} ions as a model analyte. Changing the molecular structure of the underlying Schiff base may provide selectivity to more relevant target ions. The general concept is more versatile and can provide the basis for a broad range of common specific binding concepts, from crown ethers to bioconjugate chemistry for versatile, autonomous detection of different ionic, molecular or biochemical analytes.

We thank Dr Salvatore Chiera for carrying out XPS measurements. AAB and NV acknowledge funding of the German Science Foundation (Deutsche Forschungsgemeinschaft, DFG) under grant number AN 1301/5-2 and VO 1824/5-2, respectively.

AAB and NV conceptualized the research, acquired fundings, supervised and validated the results. GM, MO, AAB and NV contributed to develop the methodology of research. GM and MO contributed to the investigation and data visualization. GM wrote the original draft. All authors contributed to its review.

Data availability

The data supporting this article have been included as part of the ESI, and the raw data can be found at **https://doi.org/10.5281/zenodo.10697663**.†

Conflicts of interest

There are no conflicts to declare.

Notes and references

1 R. Umapathi, S. Sonwal, M. J. Lee, G. Mohana Rani, E.-S. Lee, T.-J. Jeon, S.-M. Kang, M.-H. Oh and Y. S. Huh, *Coord. Chem. Rev.*, 2021, **446**, 214061.
2 M. I. Mead, O. A. M. Popoola, G. B. Stewart, P. Landshoff, M. Calleja, M. Hayes, J. J. Baldovi, M. W. McLeod, T. F. Hodgson, J. Dicks, A. Lewis, J. Cohen, R. Baron, J. R. Saffell and R. L. Jones, *Atmos. Environ.*, 2013, **70**, 186–203.
3 P. Kruse, *J. Phys. D: Appl. Phys.*, 2018, **51**, 203002.
4 S. A. Walper, G. Lasarte Aragonés, K. E. Sapsford, C. W. Brown, C. E. Rowland, J. C. Breger and I. L. Medintz, *ACS Sens.*, 2018, **3**, 1894–2024.
5 J. Kim, A. S. Campbell, B. E.-F. de Ávila and J. Wang, *Nat. Biotechnol.*, 2019, **37**, 389–406.
6 A. M. López-Marzo and A. Merkoçi, *Lab Chip*, 2016, **16**, 3150–3176.
7 S. A. Jaywant and K. M. Arif, *Sensors*, 2019, **19**, 4781.
8 N. Adarsh, M. Shanmugasundaram and D. Ramaiah, *Anal. Chem.*, 2013, **85**, 10008–10012.
9 S. Brandt, I. Pavlichenko, A. V. Shneidman, H. Patel, A. Tripp, T. S. B. Wong, S. Lazaro, E. Thompson, A. Maltz, T. Storwick, H. Beggs, K. Szendrei-Temesi, B. V. Lotsch, C. N. Kaplan, C. W. Visser, M. P. Brenner, V. N. Murthy and J. Aizenberg, *Proc. Natl. Acad. Sci. U. S. A.*, 2023, **120**, e2303928120.
10 E. Armstrong and C. O'Dwyer, *J. Mater. Chem. C*, 2015, **3**, 6109–6143.
11 D. Kou, W. Ma and S. Zhang, *Adv. Funct. Mater.*, 2021, **31**, 2007032.
12 S. A. Asher, A. C. Sharma, A. V. Goponenko and M. M. Ward, *Anal. Chem.*, 2003, **75**, 1676–1683.
13 H. Jiang, Y. Zhu, C. Chen, J. Shen, H. Bao, L. Peng, X. Yang and C. Li, *New J. Chem.*, 2012, **36**, 1051.
14 A. C. Arsenault, T. J. Clark, G. Von Freymann, L. Cademartiri, R. Sapienza, J. Bertolotti, E. Vekris, S. Wong, V. Kitaev, I. Manners, R. Z. Wang, S. John, D. Wiersma and G. A. Ozin, *Nat. Mater.*, 2006, **5**, 179–184.
15 C. G. Schäfer, M. Gallei, J. T. Zahn, J. Engelhardt, G. P. Hellmann and M. Rehahn, *Chem. Mater.*, 2013, **25**, 2309–2318.
16 J. D. Joannopoulos, S. G. Johnson and J. N. Winn, *Photonic Crystals: Molding the Flow of Light*, Princeton University Press, Princeton, NJ, 2nd edn, 2011.
17 R. C. Schroden, M. Al-Daous, C. F. Blanford and A. Stein, *Chem. Mater.*, 2002, **14**, 3305–3315.
18 B. Hatton, L. Mishchenko, S. Davis, K. H. Sandhage and J. Aizenberg, *Proc. Natl. Acad. Sci. U. S. A.*, 2010, **107**, 10354–10359.
19 K. R. Phillips, G. T. England, S. Sunny, E. Shirman, T. Shirman, N. Vogel and J. Aizenberg, *Chem. Soc. Rev.*, 2016, **45**, 281–322.
20 I. Papiano, S. De Zio, A. Hofer, M. Malferrari, I. Mínguez Bacho, J. Bachmann, S. Rapino, N. Vogel and G. Magnabosco, *Mater. Horiz.*, 2023, **10**, 4380–4388.
21 C. Chi, F. Bai, X. Xu, P. Qu, J. Xian, L. Li and D. Zhang, *Analyst*, 2022, **147**, 3486–3493.
22 Y. Yu, S. Brandt, N. J. Nicolas and J. Aizenberg, *ACS Appl. Mater. Interfaces*, 2020, **12**, 1924–1929.
23 N. J. Nicolas, M. A. Duffy, A. Hansen and J. Aizenberg, *Adv. Healthcare Mater.*, 2021, **10**, 2001326.
24 I. B. Burgess, N. Koay, K. P. Raymond, M. Kolle, M. Lon and J. Aizenberg, *ACS Nano*, 2012, **6**, 1427–1437.
25 K. P. Raymond, I. B. Burgess, M. H. Kinney, M. Lončar and J. Aizenberg, *Lab Chip*, 2012, **12**, 3666.
26 T. A. Singleton, I. B. Burgess, B. A. Nerger, A. Goulet-Hanssens, N. Koay, C. J. Barrett and J. Aizenberg, *Soft Matter*, 2014, **10**, 1325–1328.
27 I. B. Burgess, L. Mishchenko, B. D. Hatton, M. Kolle, M. Lončar and J. Aizenberg, *J. Am. Chem. Soc.*, 2011, **133**, 12430–12432.
28 A. Khalil, P. Rostami, G. K. Auernhammer and A. Andrieu-Brunsen, *Adv. Mater. Inter.*, 2021, **8**, 2100252.
29 A. M. Abu-Dief and I. M. A. Mohamed, *Beni-Suef Univ. J. Basic Appl. Sci.*, 2015, **4**, 119–133.
30 V. K. Gupta, A. K. Singh and L. K. Kumawat, *Sens. Actuators, B*, 2014, **195**, 98–108.
31 S. Q. Memon, N. Memon, A. Mallah, R. Soomro and M. Y. Khuhawar, *Curr. Anal. Chem.*, 2014, **10**, 393–417.
32 P. G. Cozzi, *Chem. Soc. Rev.*, 2004, **33**, 410–421.
33 J. Docherty, S. Mabbott, E. Smith, K. Faulds, C. Davidson, J. Reglinski and D. Graham, *Analyst*, 2016, **141**, 5857.
34 M. Strianese, D. Guarnieri, M. Lamberti, A. Landi, A. Peluso and C. Pellecchia, *Inorg. Chem.*, 2020, **59**, 15977–15986.
35 S. Goswami, *Tetrahedron Lett.*, 2013, **54**, 5075–5077.
36 K. B. Kim, G. J. Park, H. Kim, E. J. Song, J. M. Bae and C. Kim, *Inorg. Chem. Commun.*, 2014, **46**, 237–240.
37 D. Peralta-Domínguez, M. Rodríguez, G. Ramos-Ortíz, J. L. Maldonado, M. A. Meneses-Nava, O. Barbosa-García, R. Santillan and N. Farfán, *Sens. Actuators, B*, 2015, **207**, 511–517.
38 K. R. Phillips, N. Vogel, I. B. Burgess, C. C. Perry and J. Aizenberg, *Langmuir*, 2014, **30**, 7615–7620.
39 S. Li, J. M. Scheiger, Z. Wang, Z. Dong, A. Welle, V. Trouillet and P. A. Levkin, *Adv. Funct. Mater.*, 2021, **31**, 2107716.